APPLIED PHYSICS

Voltage control of unidirectional anisotropy in ferromagnet-multiferroic system

Sasikanth Manipatruni[1]*, Dmitri E. Nikonov[1], Chia-Ching Lin[1], Bhagwati Prasad[2], Yen-Lin Huang[2], Anoop R. Damodaran[2], Zuhuang Chen[2], Ramamoorthy Ramesh[2], Ian A. Young[1]

Demonstration of ultralow energy switching mechanisms is imperative for continued improvements in computing devices. Ferroelectric (FE) and multiferroic (MF) order and their manipulation promise an ideal combination of state variables to reach attojoule range for logic and memory (i.e., ~30× lower switching energy than nanoelectronics). In $BiFeO_3$ (BFO), the coupling between the antiferromagnetic (AFM) and FE order is robust at room temperature, scalable in voltage, stabilized by the FE order, and can be integrated into a fabrication process for a beyond-CMOS (complementary metal-oxide semiconductor) era. The presence of the AFM order and a canted magnetic moment in this system causes exchange interaction with a ferromagnet such as $Co_{0.9}Fe_{0.1}$ or $La_{0.7}Sr_{0.3}MnO_3$. Previous research has shown that exchange coupling (uniaxial anisotropy) can be controlled with an electric field. However, voltage modulation of unidirectional anisotropy, which is preferred for logic and memory technologies, has not yet been demonstrated. Here, we present evidence for electric field control of exchange bias of laterally scaled spin valves that is exchange coupled to BFO at room temperature. We show that the exchange bias in this bilayer is robust, electrically controlled, and reversible. We anticipate that magnetoelectricity at these scaled dimensions provides a powerful pathway for computing beyond modern nanoelectronics by enabling a new class of nonvolatile, ultralow energy computing elements.

INTRODUCTION

The exponential scaling in computing device density and concurrent gains in the efficiency of computation relies on reducing the device-level switching energy (*1*–*3*). Among the various switching devices, ferroelectric (FE) and multiferroic (MF) (*4*, *5*) devices allow energy efficient electronics (*6*, *7*). In multiferroic $BiFeO_3$ (BFO), the coupling between the antiferromagnetic (AFM) and FE order is robust at room temperature (*8*, *9*) with potentially low switching voltages (*10*) and integration path for microelectronics (*11*, *12*). The presence of the AFM order and a canted magnetic moment in this system (*13*) causes exchange interaction with a ferromagnet such as $Co_{0.9}Fe_{0.1}$ (*14*, *15*) or $La_{0.7}Sr_{0.3}MnO_3$ (LMSO) (*16*). Nanoelectronics has entered an exciting and yet challenging phase in which the transistor dimensions have already been scaled down to ~10 nm (*17*). Further, device-level improvements are likely to involve new physical mechanisms and new state variables (*18*). In this context, the discovery and development of novel devices suitable for computing have become imperative. Magnetoelectric switching provides a new and potentially ultralow energy switching mechanism, since the energy density for switching [Energy/Area (E/A) = $2 \cdot P_C \cdot V_{FE}$, where P_c is the polarization per unit area and V_{FE} is the FE switching voltage] can be scaled to 1 μJ/cm^2, a 30 to 100× leap in energy efficiency compared to modern complementary metal-oxide semiconductor ($E/A = {}^1/_2\, C \cdot V^2$, where C is the capacitance per unit area). Further, the MF nature of the switching medium enables nonvolatility (relying on the FE polarization $\boldsymbol{P}$ and the AFM order $\boldsymbol{L}$), directionality, and signal regeneration. Magnetoelectric MF can enable *aJ* class logic and memory (*7*, *19*), where a voltage-driven MF switches the magnetization of a ferromagnet (Fig. 1).

The preferred magnetoelectric switching method for device applications is the presence of an electrically controllable exchange bias to switch a FM in direct contact with the MF. While spin-torque–driven switching of a FM has been well studied, showing the existence of both field- and damping-like torques (*20*, *21*), magnetoelectric switching torques on a ferromagnet due to a magnetoelectric MF have not been described. Electrically controllable exchange bias (EB) (i) modifies the energy landscape of the magnet asymmetrically, whereas exchange coupling (EC) produces a uniaxial change to the magnetization landscape (Fig. 1, B and C); and (ii) allows wider range/independent switching dynamics for the FM in a logic/memory device. Ab initio studies of the MF BFO (*22*–*24*) suggest that within a single FE domain, there exists the possibility of a directional magnetic coupling, that is, the possibility of an electrically switchable exchange bias, due to the presence of the canted magnetization (*25*–*30*). The MF can therefore impose an electric field–controllable exchange bias onto a ferromagnet that is in contact with it. Prior work on BFO, the only reliably high-temperature magnetoelectric MF (*13*–*15*), has shown the ability to control the direction of magnetization in a FM layer via exchange coupling to the MF surface. In particular, work by Heron (*14*) demonstrates reversible FM switching with a MF, in the absence of a magnetic field, through the application of an electric field to the CoFe/BFO heterostructure. However, a reversible exchange bias modulation has not been experimentally described. Electrical control of exchange bias with MFs has been limited to low temperatures (*31*), with LSMO as the ferromagnet. Cr_2O_3 (*32*) exhibits a robust exchange bias but lacks the FE order. That makes an external magnetic field necessary for switching, limiting its nonvolatility and suitability for device applications.

In this work, we demonstrate that there is a robust, electrically switchable exchange bias at the interface between the BFO layer and a dimensionally scaled CoFe/Cu/CoFe giant magnetoresistance (GMR) spin valve. A key to the observation of the exchange bias appears to be the reduction in the lateral dimensions of the GMR stack, with respect to the FE domains in the BFO layer. Furthermore, this exchange bias is reversibly modulated by a bipolar electric field, again confirming the directional coupling of magnetism and its control with an electric field. Thus, electrically controllable exchange bias is a key

[1]Components Research, Intel Corp., Hillsboro, OR 97124, USA. [2]Department of Materials Science and Engineering and Department of Physics, University of California, Berkeley, CA 94720, USA.
*Corresponding author. Email: sm448@cornell.edu

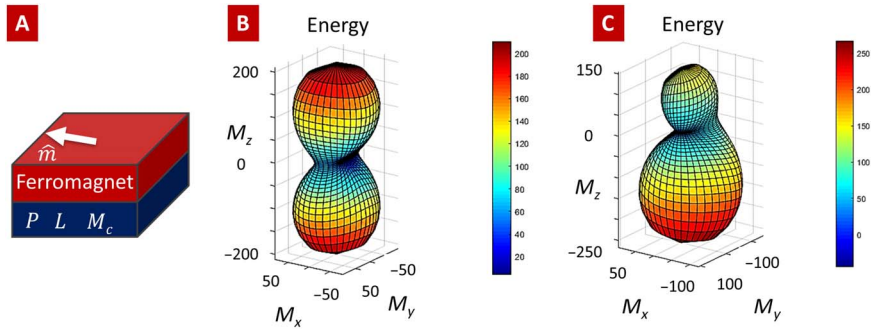

Fig. 1. Interaction of a FM with a multiferroic. (**A**) Energy landscape of a ferromagnet interacting with a MF. (**B**) Exchange coupling only (symmetric about the in-plane hard axis). (**C**) Exchange bias and coupling (asymmetric about the hard axis). Exchange bias breaks the spatial symmetry in the energy landscape. This breaking of symmetry by exchange bias is similar to applying an external magnetic bias.

enabler for a new class of logic and memory devices for reducing the energy per transition of a solid-state switch beyond the modern nanoelectronic transistors.

The description of the magnetoelectric switching torques (from exchange bias and exchange coupling) in a magnetoelectric switch is a critical first step for using this phenomenon. If a ferromagnet with magnetization M_{FM} is coupled to a magnetoelectric MF and antiferromagnet (where M_1 and M_2 are the moments of the magnetic sublattices of the antiferromagnet), the coupling is most conveniently expressed via the uncompensated magnetization due to canting of the sublattice moments $M_c = M_1 + M_2$, and the AFM order $L = M_1 - M_2$. The switching of the ferromagnet can be described by the Landau-Lifshitz-Gilbert (*33*) equation modified with magnetoelectric coupling (ME-LLG) terms

$$\frac{\partial m_{FM}}{\partial t} = -\gamma\mu_0\left[m_{FM} \times \vec{H}_{eff}\left(\vec{L}, \vec{M}_c\right)\right] + \alpha\left[m_{FM} \times \frac{\partial m_{FM}}{\partial t}\right] \quad (1)$$

where the effective field includes the contributions from shape anisotropy ($\vec{H}_{sh}$), magnetocrystalline anisotropy ($\vec{H}_{mcry}$), exchange coupling ($\vec{H}_{ec}$), and exchange bias ($\vec{H}_{eb}$)

$$\vec{H}_{eff} = \vec{H}_{sh} + \vec{H}_{mcry} + \vec{H}_{ec} + \vec{H}_{eb}$$
$$\vec{H}_{ec}(\vec{L}) = H_{ec}\hat{l}(\hat{l}\cdot\hat{m}_{FM})$$
$$\vec{H}_{eb}(\vec{M}_c) = H_{eb}\hat{m}_c \quad (2)$$

Here, lowercase letters with hats denote unit vectors along the corresponding upper case vectors. Furthermore, $\vec{H}_{ec}(\vec{L})\bullet\vec{H}_{eb}(\vec{M}_c) = 0$ $\hat{L}\bullet\hat{m}_c = 0$ for equivalent sublattices. It is known that in BFO, vectors ***P***, ***L***, and $\boldsymbol{M_c}$ undergo a kinetic two-step process in response to an electric field (please see Fig. 2 and section S1) (*14*). Figure 2 shows the trajectory of ***L*** and $\boldsymbol{M_c}$, following the trajectory of the polarization ***P***, where ***P*** undergoes a non-Vanderbilt switching mechanism (where the ***P*** rotates, avoiding a zero-polarization state). Accordingly, $\boldsymbol{M_c}$ produces a reversible exchange bias when ***P*** is reversed via application of out-of-plane voltage. The torque arising due to coupling to antiferromagnetism (τ_L, T_{AFM}) and torque due to coupling to canted ferromagnetism $\boldsymbol{M_c}$ (τ_{Mc}, T_{Mc}) affect the ferromagnet in different ways: τ_L produces a steady-state anisotropy change (exchange coupling), and τ_{Mc} produces a steady-state effective directional magnetic field (exchange bias). If τ_{Mc} is stronger than the combination of anisotropies, then it can cause magnetization reversal. Exchange bias torque, τ_{Mc}, defines a switching trajectory for the FM, so it does not need to respond in a time scale close to the FE time scale. In particular, for (001) lattice orientation of the BFO film, τ_{Mc} can also exert an out-of-plane torque due to an out-of-plane projection of the canted magnetic moment. In addition, magnetization reversal can result from τ_L, provided that the magnet responds on a time scale faster than the FE switching time scale; then, the magnetization is able to follow the rotation of the ***L*** vector (see Table 1).

We have fabricated ferromagnet-MF heterostructure devices comprising current in-plane GMR (CIP-GMR) lateral spin valves ($Co0_{0.9}Fe_{0.1}$/Cu/$Co_{0.9}Fe_{0.1}$) coupled to the MF BFO (see Materials and Methods for device processing details) (fig. S1). We deposit MF $(001)_p$ BFO (100 nm) on a conducting layer $SrRuO_3$ (20 nm) on a (110) $DyScO_3$ substrate. $DyScO_3$ substrates provide an anisotropic strain in the BFO film and allow only two of the eight stable polarizations of the BFO [Fig. 3 (E and F) shows the PFM imaging of the two-variant BFO]. We use an electrode on the periphery of the chip to make contact to the $SrRuO_3$ conductive back electrode for the application of an out-of-plane electric field for polarization switching. A GMR stack is deposited in situ on the BFO under ultrahigh vacuum conditions to provide a direct sensing mechanism for the state of the electrically controlled bottom magnet. Three sets of test chips were processed, comprising more than 1000 ME-GMR devices, which comprised GMR stripes at angles of 0°, 45°, 90°, and 135° with respect to the FE domains in the BFO (which lie along the pseudo-cubic $[100]_{pc}$ directions).

RESULTS

Using the sensitive and local CIP-GMR magnetotransport measurements, we observe a magnetically stable exchange bias in devices with lateral dimensions ~200 nm (among the smallest devices made in our study). The exchange bias is manifested as an asymmetry in the resistance versus applied magnetic field (*R*-*H*) hysteresis. The exchange bias is stable at room temperature with respect to magnetic cycling and progressively becomes stronger as the lateral dimensions are decreased below ~1 to 2 μm (Fig. 3, A and B). This observation is consistent with the local exchange bias observed in other systems, namely Py/$YMnO_3$ (*27*) and Co/LaFeO3 (*28*), which show dimension-dependent exchange bias (*29*). To understand the fundamental origins of how the exchange bias emerges as the lateral dimensions are reduced, we carried out detailed micromagnetic simulations of the GMR stack, with various boundary conditions imposed on the stack. The micromagnetic (see Materials and Methods) effect of exchange coupling due to the AFM order of BFO (***L***) and exchange bias due to canted magnetization ($\boldsymbol{M_C}$) is shown in fig. S2 and

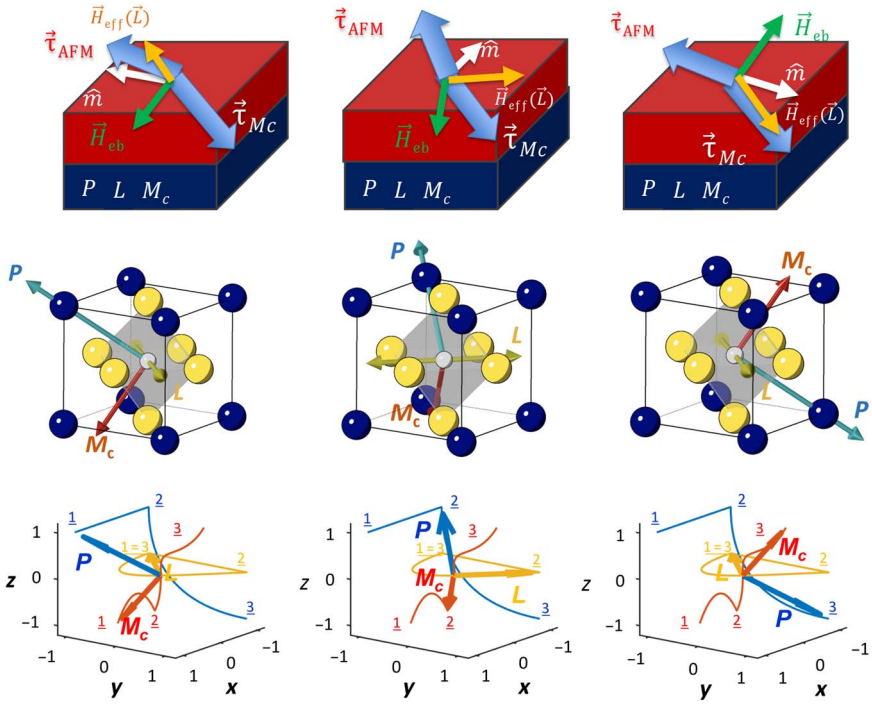

Fig. 2. Geometry of magnetoelectric switching in the BFO/CoFe interface. Top: Stack of BFO (blue) and CoFe (dark red) layers. Directions of magnetization ($\hat{m}$), effective magnetic field of exchange bias (H_{eb}) and of exchange coupling ($H_{eff}(L)$), torques due to exchange bias (τ_{Mc}) and exchange coupling (τ_{AFM}) are shown. Initial state where τ_L, T_{AFM} and τ_{Mc}, T_{MC} and torque due to anisotropy produce a net zero ME torque. Intermediate state where the τ_L, T_{AFM} and τ_{Mc}, T_{MC} are driving the FM dynamics due to the intermediate polarization switching state of BFO final state, where τ_L, T_{AFM} and τ_{Mc}, T_{MC}, and torque due to anisotropy produce a net zero ME torque, $\boldsymbol{M_c} = \boldsymbol{M_1} + \boldsymbol{M_2}$, and $\boldsymbol{L} = \mathbf{M_1} - \mathbf{M_2}$ experience 180° reversal. **Middle:** The directions of *P*, *L*, and M_c are shown relative to the crystal axes. **Bottom**: Trajectories of *P*, *L*, and M_c relative to the crystal axes. In columns: Three special states in the switching process: the initial, after a 71° turn of polarization, and the final, after a 109° turn.

Table 1. Comparisons of the two factors in the magnetoelectric switching, AFM exchange coupling, and exchange bias.

Magnetoelectric switching torques	AFM torque	Exchange bias torque
Origin	Coupling to *L* of BFO	Coupling to M_c of BFO
Directionality/symmetry	Uniaxial anisotropy (L^2) $\bar{H}_{eff}(\vec{L}) = \bar{H}_{eff} + H_e\hat{L}(\hat{L}\cdot\hat{m})$	Unidirectional anisotropy (M_c) $\bar{H}_{eb}(\vec{M}_c)$
Steady state	Produces anisotropy enhancement in the GMR/AMR devices	Produces exchange bias in the GMR and AMR transport measurements
FM switching	Kinetic rotation. FM undergoes a kinetic process (multistep) with the ME for 180° switching, where it follows the ***L*** vector	FM can undergo an independent switching trajectory, independent of the ME/FE switching dynamics
Direction of the effective field	Exerts an in-plane effective field (in the direction of the ***L*** vector)	Exerts a canted effective field with an out-of-plane component (in the direction of M_c)

compared with magnetic force microscopy images. All of the physical interaction parameters, such as the strength of exchange bias and the anisotropy, were kept unchanged, with the only variable being the lateral dimension of the ME-GMR element. The central results of our simulations of the GMR response as a function of magnetic field for the two lateral length scales studied are shown in Fig. 3 (C and D). Consistent with the experimental data in Fig. 3 (A and B), the simulations also show an enhanced asymmetry of the 200-nm-wide GMR devices; this asymmetry progressively decreases as the lateral dimension is increased such that the 2000-nm (2 μm) devices show negligible shift. Factors relevant for switching are presented in the micromagnetic simulations: demagnetization, including dipole interaction between the top and bottom layers, material anisotropy, exchange stiffness, and external magnetic field. In addition, coordinate-dependent (due to stripe domains) exchange bias (effective field) and exchange coupling (in-plane anisotropy) act on the bottom layer.

To understand the possible origins of this interesting lateral size dependence of the unidirectional coupling, we performed micromagnetic simulations of the magnetoelectric exchange interaction with the GMR stack to establish both the presence of a unidirectional anisotropy—exchange bias and the effect of electrical switching of this exchange bias. These simulations with locally modulated exchange interactions following the MF domain pattern were performed for (i) comparing ME-GMR device sizes (2000 nm by 200 nm in fig. S3

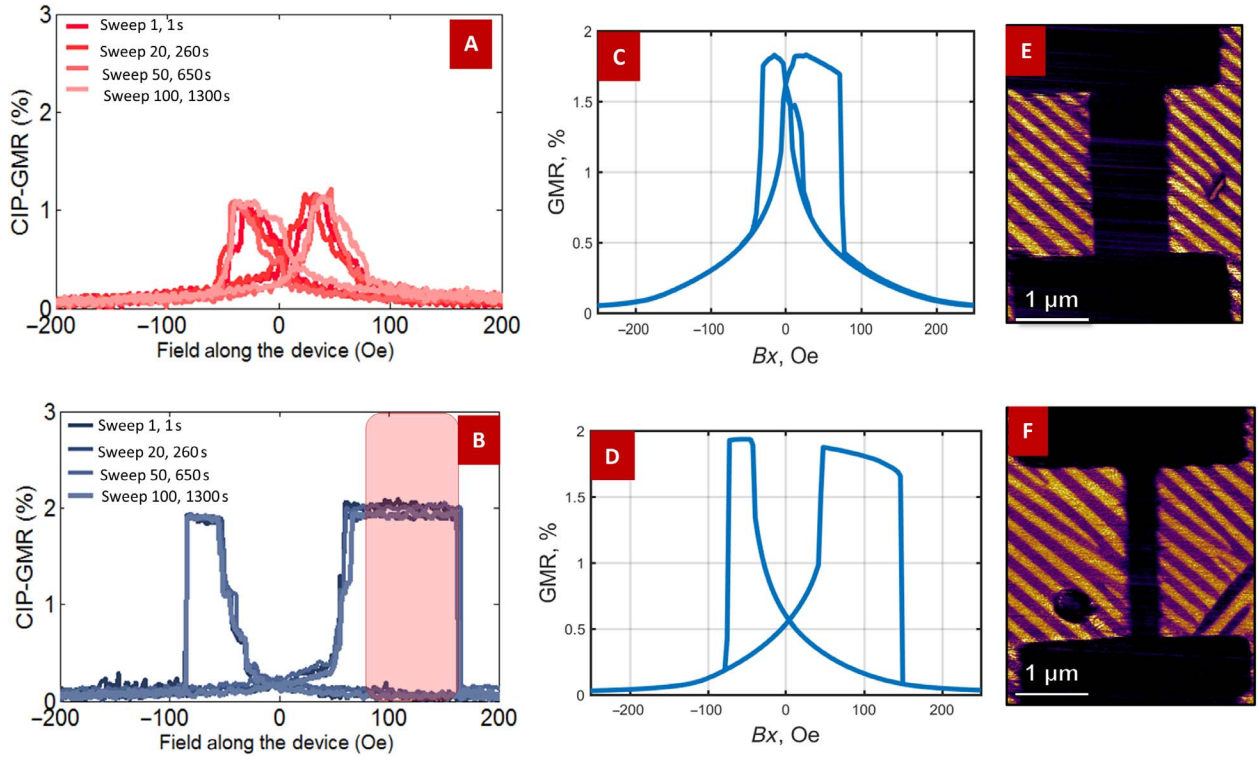

Fig. 3. Exchange bias in ME-GMR devices. Magnetotransport measurement of an ME-GMR device (geometry and cross section are shown in fig. S2) fabricated on a two-variant MF BFO with (**A**) lateral dimensions 1 μm by 2 μm and (**B**) lateral dimensions 200 nm by 2 μm. Micromagnetic simulation of the ME-GMR device comprehending the exchange bias and exchange coupling from MF substrates (**C**) for lateral dimensions 1 μm by 2 μm and (**D**) 200 nm by 2 μm. Piezoelectric force microscopy (PFM) images of the devices for dimensions (**E**) 1 μm by 2 μm and (**F**) 200 nm by 2 μm. Scaled devices show the presence of an exchange bias exerted on the FM layer in contact with BFO. (A) and (B) show the magnetic transport measurement repeated for 100 cycles (1300 s).

and 2000 nm by 1000 nm in fig. S4), (ii) reversal of the sign of exchange bias (fig. S5), and (iii) effect of domain orientation with respect to the ME-GMR device [45° orientation of ME-GMR with respect to MF domains (fig. S3) and 135° orientation of ME-GMR with respect to MF domains (fig. S6)]. The results of the simulations show close agreement with the experimental magnetotransport data. The resulting net magnetization reversal of a 2000 nm by 200 nm spin valve layer in contact with the BFO is shown in fig. S3, and that for a 2000 nm by 1000 nm device is shown in S4. The magnetic patterns of the BFO are also visible in the top GMR layer because of exchange and dipole interactions within the CIP-GMR stack. In the presence of the exchange bias, the magnetization hysteresis and correspondingly magnetoresistance (*R-H*) show asymmetry around zero field, which is qualitatively different as the lateral dimensions are reduced. For wires of 2000 nm by 200 nm, the simulations reveal two key features, namely (i) a large unidirectional anisotropy in the switching field, that is, an exchange bias manifested as a shift of the hysteresis for the bottom CoFe layer and, consequently, to asymmetric *R-H* hysteresis loops. In addition to this, due to the shape anisotropy of this test structure, the top CoFe layer exhibits a larger coercivity. As the magnetization switches with an external magnetic field, the magnetization in both layers remains approximately aligned along the FM wire, although with significant local deviations where it is forced by exchange coupling to BFO (see figs. S3 to S6). The switching to mostly the opposite direction happens as a sudden transition relative to the external field. We attribute this as the main reason for the sharp steps in the *R-H* hysteresis at well-separated values of the applied field. In contrast, for the wires of 2000 nm by 1000 nm, shape anisotropy plays an insignificant role. In other words, we identify the large asymmetry of *R-H* hysteresis in wires narrower than the width of BFO domains (with lack of asymmetry in wider wires) as a signature of the exchange bias. In structures with larger lateral dimensions, there is an averaging effect of the canted moment in each domain, and consequently, the exchange bias progressively becomes weaker.

DISCUSSION

Armed with this critical insight that the lateral dimensions play a key role in the emergence of a measurable exchange bias (*28*), we then proceeded to ask: Can this exchange bias be modulated with an applied electric field that switches the polarization of BFO (*29*, *30*)? The electrical control of the BFO is obtained via contacts to a conductive oxide bottom electrode formed with $SrRuO_3$. The voltage-controlled GMR hysteresis for the devices is shown in Fig. 4. The GMR hysteresis of the electrically pristine devices (i.e., devices before the first FE switching was made) is shown in Fig. 4A. A reversible exchange bias is observed with the application of an electric pulse (10 μs long with a current limit of 10 μA). The two hysteresis loops indicate the magnetic switching of the bottom FM and top FM. The bottom FM has an enhanced magnetic anisotropy and switches at higher magnetic fields. In contrast, the top FM has a lower anisotropy. We observe that the sign of the magnetoelectric tuning of the hysteresis curves is consistent with a unidirectional anisotropy. Micromagnetic simulations with exchange coupling following the MF domain pattern are consistent with the reversal of exchange

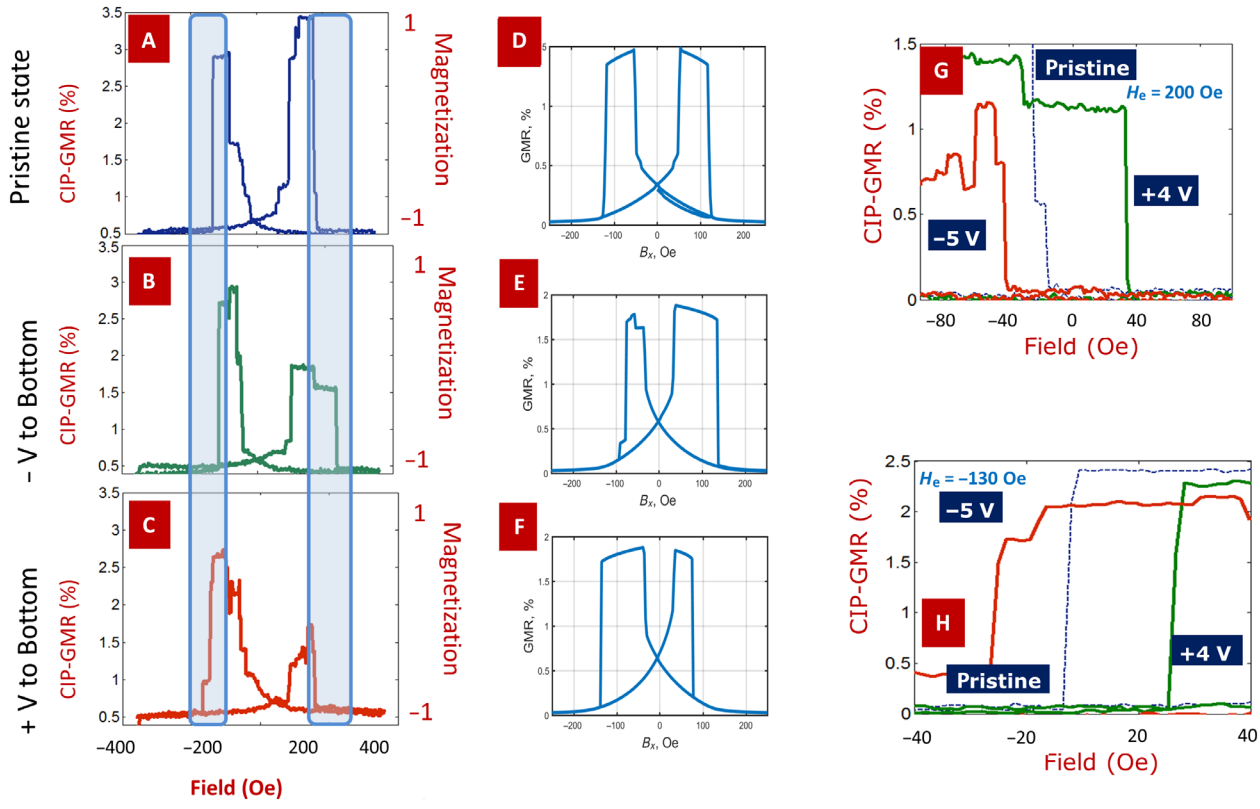

Fig. 4. Reversible exchange bias in magnetoelectric GMR devices. (**A**) Prestine GMR devices before first switching of ferroelectricity showing no asymmetry in the GMR transport. (**B**) ME-GMR with negative exchange bias, which produces a higher positive switching field. (**C**) ME-GMR with positive exchange bias, which produces a higher negative switching field for the contact ferromagnet. Micromagnetic simulation of ME-GMR devices (**D**) without exchange bias before first FE switching of the device (**E**) with negative exchange bias (see fig. S5), (**F**) with positive exchange bias (see fig. S4). (**G**) ME-GMR measurement with an external applied field of 200 Oe. (**H**) ME-GMR measurement with an external applied field of −130 Oe. Shift in switching field of the FM in contact with BFO is consistent with voltage control of the exchange bias.

bias uniaxial anisotropy. In figs. S3 and S5, a consistent magnetotransport signature is observed, where the exchange bias reverses orientation when the FE polarization undergoes 180° reversal from [1,−1,1] to [−1,1,−1] (figs. S3 and S5). However, the AFM order (L) that is an axial quantity remains unchanged. We further compare the magnetotransport trends with the micromagnetic simulations (Fig. 4, D to F) where a reversible unidirectional exchange anisotropy is applied to the free (bottom) layer (figs. S3 and S5). To highlight the effect of the electric field on the exchange bias, we centered the GMR hysteresis with an external field; for an external centering field of 200 Oe and for positive/negative voltages, the switching field is enhanced/reduced. In contrast, when the centering field is reversed, the positive/negative voltages induce a reduction/enhancement of the switching fields. We note that this can be carried out reversibly for at least 100 switching cycles. This direct relationship between the polarity of the applied electric field and the exchange bias magnitude is perhaps the most important discovery in this work, since it directly demonstrates that the canted moment in the BFO is being switched by 180° by the application of an out-of-plane electric field.

We show magnetoelectric hysteresis loops of the MF/ferromagnet heterostructure, with voltage as the independent control signal and magnetization sensed with CIP-GMR as the output. The electrical test structure is shown in fig. S1. The ME-GMR device is formed by a ferromagnet-MF heterostructure devices composed of CIP-GMR lateral spin valves ($Co_{0.90}Fe_{0.10}$/Cu/$Co_{0.90}Fe_{0.10}$) coupled to MF BFO (see Materials and Methods for device fabrication processes). The magnetoelectric transfer function with voltage is seen in Fig. 5A. Here, we apply a switching voltage pulse to the bottom electrode of the ME-GMR test structure and measure the state of the magnet. We also measure the FE polarization as a function of the applied voltage (Fig. 5B). This ME-GMR hysteresis closely resembles the FE hysteresis. The magnitude of the electrically switched GMR hysteresis matches the GMR hysteresis via magnetic sweeps, indicating a full 180° reversal of the FM layer in contact with BFO with respect to the top FM layer.

A direct consequence of a unidirectional anisotropy is the ability to project the exchange bias along a given vector, in contrast to uniaxial anisotropy. To test this hypothesis, we have fabricated devices with orientation at 45° and 135° to the striped domains on the BFO/SRO/DSO (BFO/$SrRuO_3$/$DyScO_3$) substrate (Fig. 5, C and E). Here, the easy axis (length direction) of the ME-GMR device is aligned at 45° and 135° with respect to the BFO domain topology. We expect that a unidirectional exchange bias will project as a vector producing B_{ex} proportional to cos(θ) and cos(180° − θ). Figure 5 (D and F) demonstrates that the magnetoelectric effect (exchange bias with respect to the applied electric field) reverses direction, consistent with a unidirectional effect. We have further confirmed the effect of orientation with respect to the MF domains via micromagnetic simulations (compare figs. S3 and S6). The asymmetry caused by the projection of the exchange bias along the easy axis of the device is reproduced in micromagnetics, confirming that exchange bias due to interaction of

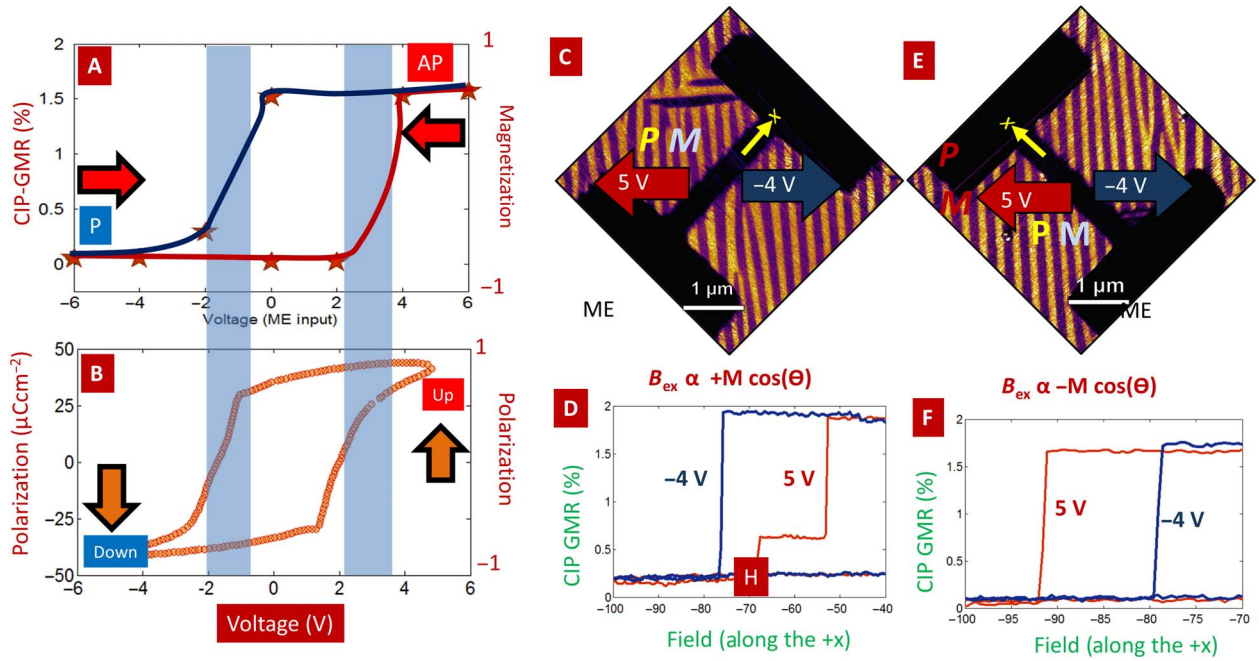

Fig. 5. Switching of magnetization by voltage. (**A**) Magnetoelectric-controlled GMR hysteresis showing full GMR switching of the device. (**B**) FE hysteresis loop of the test structure. We note that the ME-GMR and PE loops have similar switching voltages. (**C**) ME-GMR devices fabricated at an orientation of +45° w.r.t. to striped domains of BFO. (**D**) Magnetoelectric tuning of the ME-GMR stucture shown in (C). (**E**) ME-GMR devices fabricated at an orientation of 135° with respect to striped domains of BFO. (**F**) Magnetoelectric tuning of the ME-GMR structure shown in (E).

the FM with the BFO projects like a vector, with sign reversal when the projection direction changed (fig. S6). Hence, we see a reversal in the sign of the magnetoelectricity, depending on the orientation of the device with respect to the striped domains.

In conclusion, we observed a unidirectional exchange bias in a FM in contact with a room temperature MF that is electrically switchable. An electrically controlled unidirectional exchange bias interacts with the magnet similar to a directional magnetic field and opens the possibility for a wider range of logic and memory devices. The direct relationship between the polarity of the applied electric field and the exchange bias is an important discovery, since it indicates that the uncompensated magnetization (canted moment in the BFO) is being switched by 180° by the application of an out-of-plane electric field. In contrast to a magnetoelectric antiferromagnet (such as Cr_2O_3), where the switching of the magnetic state is accomplished by the simultaneous application of a magnetic field (~1000 Oe) and an electric field, in the case of a MF such as BFO, the internal field in the BFO (in the form of the canted moment) couples to the ferromagnet and thus is able to switch it with an electric field. Demonstration of a local and directional magnetoelectric switching mechanism can enable a wider class of logic/memory devices (*34*). We expect that the strength of the FM and MF interactions and magnetic switching to be improved with dimensional scaling and improved material quality. The ability to switch a nanomagnet with a locally reversible exchange field can enable a wide application space in memory and logic.

MATERIALS AND METHODS

Sample growth and process flow

In this study, 20-nm (001) $SrRuO_3$/100-nm (001) BFO was grown by pulsed-laser deposition using a KrF laser onto single-crystalline (110) $DyScO_3$ substrate. A striped FE domain structure with two polarization variants of the 100-nm BFO film was confirmed by PFM. A conducting 20-nm $SrRuO_3$ acted as a back electrode. Next, a GMR stack (2.5-nm $Co_{0.9}Fe_{0.1}$/5-nm Cu/2.5-nm $Co_{0.9}Fe_{0.1}$/2-nm Pt) was deposited by direct-current magnetron sputtering onto the 100-nm BFO film. A 2-nm Pt layer acted as a capping layer to prevent oxidation of other layers underneath. The GMR device was fabricated to study the voltage-controlled magnetoelectric switching. The final device structure is shown in fig. S1.

Micromagnetic simulations

Micromagnetic simulations were performed using the NIST (National Institute of Standards and Technology) simulator OOMMF (Object Oriented MicroMagnetic Framework). The input scripts for simulations are available among the Supplementary Materials. The following parameters were chosen to model the device: M_s = 1 MA/m is the magnetization of CoFeB, A_x = 10 pJ/m is the exchange stiffness, K_z = 200 kJ/m^3 is the uniaxial anisotropy in the top layer, w_s = 200nm is the period of striped domains, K_{ec} = 16kJ/m^3 is the in-plane anisotropy in the bottom layer due to the exchange coupling, and t_b is the thickness of the bottom layer. The patterns of exchange coupling axes and of exchange bias direction are shown in fig. S2E.

Magnetization is calculated by minimizing the overall energy of the system at every value of the external magnetic field. The magnetic field was swept from H = 300 Oe to H = − 300 Oe and back.

Magnetoelectric switching dynamics with exchange bias versus exchange coupling

In exchange coupling–mediated magnetoelectric switching, the switching dynamics of the FM have to closely follow the switching dynamics of the MF. This is due to the uniaxial nature of the exchange coupling. In

contrast, exchange bias–mediated magnetoelectric switching decouples the switching dynamics of the ferromagnet from the switching dynamics of the MF.

SUPPLEMENTARY MATERIALS

Supplementary material for this article is available at http://advances.sciencemag.org/cgi/content/full/4/11/eaat4229/DC1

Section S1. Physics of exchange bias.
Section S2. Micromagnetic simulation of a GMR device interacting with multiferroic BFO.
Section S3. Input script for the OOMMF simulator.
Fig. S1. Patterned device geometry.
Fig. S2. Micromagnetic simulation of a GMR device interacting with multiferroic BFO.
Fig. S3. Magnetization patterns in the hysteresis loop for devices of 2000 nm by 200 nm area, an applied voltage of 5 V, and an exchange bias H_{eb} = 30 Oe.
Fig. S4. Effect of ferromagnet width for a devices of 2000 nm by 1000 nm area and an exchange bias H_{eb} = 30 Oe.
Fig. S5. Switching of exchange bias sign for a devices of 2000 nm by 200 nm area, an applied voltage of −4 V, and an exchange bias H_{eb} = −30 Oe.
Fig. S6. Effect of domain orientation in BFO for a devices of 2000 nm by 200 nm area, an applied voltage of 5 V, and an exchange bias H_{eb} = −30 Oe (due to a different orientation of the electric field and the magnetic field (x = axis).
References (*35*, *36*)

REFERENCES AND NOTES

1. K. J. Kuhn, Considerations for ultimate CMOS scaling. *IEEE Trans. Electron Dev.* **59**, 1813–1828 (2012).
2. I. Ferain, C. A. Colinge, J.-P. Colinge, Multigate transistors as the future of classical metal-oxide-semiconductor field-effect transistors. *Nature* **479**, 310–316 (2011).
3. J. D. Meindl, Q. Chen, J. A. Davis, Limits on silicon nanoelectronics for terascale integration. *Science* **293**, 2044–2049 (2001).
4. D. Khomskii, Trend: Classifying multiferroics: Mechanisms and effects. *Physics* **2**, 20 (2009).
5. N. A. Spaldin, M. Fiebig, The renaissance of magnetoelectric multiferroics. *Science* **309**, 391–392 (2005).
6. S. Salahuddin, S. Datta, Use of negative capacitance to provide voltage amplification for low power nanoscale devices. *Nano Lett.* **8**, 405–410 (2008).
7. S. Manipatruni, D. E. Nikonov, R. Ramesh, H. Li, I. A. Young, Spin-orbit logic with magnetoelectric nodes: A scalable charge mediated nonvolatile spintronic logic; arXiv:1512.05428 (2015).
8. J. F. Scott, Room-temperature multiferroic magnetoelectrics. *NPG Asia Mater.* **5**, e72 (2013).
9. J. Wang, J. B. Neaton, H. Zheng, V. Nagarajan, S. B. Ogale, B. Liu, D. Viehland, V. Vaithyanathan, D. G. Schlom, U. V. Waghmare, N. A. Spaldin, K. M. Rabe, M. Wuttig, R. Ramesh, Epitaxial $BiFeO_3$ multiferroic thin film heterostructures. *Science* **299**, 1719–1722 (2003).
10. Y. H. Chu, Q. Zhan, C.-H. Yang, M. P. Cruz, L. W. Martin, T. Zhao, P. Yu, R. Ramesh, P. T. Joseph, I. N. Lin, W. Tian, D. G. Schlom, Low voltage performance of epitaxial $BiFeO_3$ films on Si substrates through lanthanum substitution. *Appl. Phys. Lett.* **92**, 102909 (2008).
11. S. Beyer, M. Trentzsch, S. Flachowsky, R. Richter, J. Paul, B. Reimer, D. Utess, S. Jansen, H. Mulaosmanovic, S. Müller, S. Slesazeck, J. Ocker, M. Noack, J. Müller, P. Polakowski, J. Schreiter, S. Beyer, T. Mikolajick, B. Rice, A 28nm HKMG super low power embedded NVM technology based on ferroelectric FETs, in *2016 IEEE International Electron Devices Meeting (IEDM)*, San Francisco, CA (2016), pp. 11.5.1–11.5.4.
12. C. Ederer, N. A. Spaldin, Weak ferromagnetism and magnetoelectric coupling in bismuth ferrite. *Phys. Rev. B* **71**, 060401(R) (2005).
13. J. T. Heron, J. L. Bosse, Q. He, Y. Gao, M. Trassin, L. Ye, J. D. Clarkson, C. Wang, J. Liu, S. Salahuddin, D. C. Ralph, D. G. Schlom, J. Íñiguez, B. D. Huey, R. Ramesh, Deterministic switching of ferromagnetism at room temperature using an electric field. *Nature* **516**, 370–373 (2014).
14. J. T. Heron, M. Trassin, K. Ashraf, M. Gajek, Q. He, S. Y. Yang, D. E. Nikonov, Y.-H. Chu, S. Salahuddin, R. Ramesh, Electric-field-induced magnetization reversal in a ferromagnet-multiferroic heterostructure. *Phys. Rev. Lett.* **107**, 217202 (2011).
15. M. Trassin, J. D. Clarkson, S. R. Bowden, J. Liu, J. T. Heron, R. J. Paull, E. Arenholz, D. T. Pierce, J. Unguris, Interfacial coupling in multiferroic/ferromagnet heterostructures. *Phys. Rev. B* **87**, 134426 (2013).
16. L. You, B. Wang, X. Zou, Z. S. Lim, Y. Zhou, H. Ding, L. Chen, J. Wang, Origin of the uniaxial magnetic anisotropy in $La_{0.7}Sr_{0.3}MnO_3$ on stripe-domain $BiFeO_3$. *Phys. Rev. B* **88**, 184426 (2013).
17. S. Natarajan, M. Agostinelli, S. Akbar, M. Bost, A. Bowonder, V. Chikarmane, S. Chouksey, A. Dasgupta, K. Fischer, Q. Fu, T. Ghani, M. Giles, S. Govindaraju, R. Grover, W. Han, D. G. Hanken, E. Haralson, M. Haran, M. Heckscher, R. Heussner, P. Jain, R. James, R. Jhaveri, I. Jin, H. Kam, E. Karl, C. L. Kenyon, M. Y. Liu, Y. Luo, R. Mehandru, S. Morarka, L. Neiberg, P. Packan, A. Paliwal, C. Parker, P. Patel, R. Patel, C. Pelto, L. C. Pipes, P. Plekhanov, M. Prince, S. Rajamani, J. Sandford, B. Sell, S. Sivakumar, P. Smith, B. Song, K. Tone, T. Tröger, J. Wiedemer, M. Yang, K. Zhang, A 14nm logic technology featuring 2nd-generation FinFET, air-gapped interconnects, self-aligned double patterning and a 0.0588 μm2 SRAM cell size, in *2014 IEEE International Electron Devices Meeting (IEDM)* (IEEE, 2014), pp. 3–7.
18. D. E. Nikonov, I. A. Young, Benchmarking of beyond-CMOS exploratory devices for logic integrated circuits, in *IEEE Journal on Exploratory Solid-State Computational Devices and Circuits* (2015), vol. 1, pp. 3–11.
19. N. X. Sun, G. Srinivasan, Voltage control of magnetism in multiferroic heterostructures and devices. *Spin* **2**, 1240004 (2012).
20. J. C. Sankey, Y.-T. Cui, J. Sun, J. C. Slonczewski, R. A. Buhrman, D. C. Ralph, Measurement of the spin-transfer-torque vector in magnetic tunnel junctions. *Nat. Phys.* **4**, 67–71 (2008).
21. H. Kubota, A. Fukushima, K. Yakushiji, T. Nagahama, S. Yuasa, K. Ando, H. Maehara, Y. Nagamine, K. Tsunekawa, D. D. Djayaprawira, N. Watanabe, Y. Suzuki, Quantitative measurement of voltage dependence of spin-transfer torque in MgO-based magnetic tunnel junctions. *Nat. Phys.* **4**, 37–41 (2008).
22. J. C. Wojdeł, J. Íñiguez, Magnetoelectric response of multiferroic $BiFeO_3$ and related materials from first-principles calculations. *Phys. Rev. Lett.* **103**, 267205 (2009).
23. M. Stengel, J. Íñiguez, Electrical phase diagram of bulk $BiFeO_3$. *Phys. Rev. B* **92**, 235148 (2015).
24. D. L. Vinokurov, A. I. Morosov, Magnetic structure of the compensated ferromagnet-multiferroic interface. *Phys. Solid State* **55**, 2246–2251 (2013).
25. H. Béa, M. Bibes, F. Ott, B. Dupé, X.-H. Zhu, S. Petit, S. Fusil, C. Deranlot, K. Bouzehouane, A. Barthélémy, Mechanisms of exchange bias with multiferroic $BiFeO_3$ epitaxial thin films. *Phys. Rev. Lett.* **100**, 017204 (2008).
26. A. P. Malozemoff, Random-field model of exchange anisotropy at rough ferromagnetic-antiferromagnetic interfaces. *Phys. Rev. B* **35**, 3679(R) (1987).
27. V. Laukhin, V. Skumryev, X. Martí, D. Hrabovsky, F. Sánchez, M. V. García-Cuenca, C. Ferrater, M. Varela, U. Lüders, J. F. Bobo, J. Fontcuberta, Electric-field control of exchange bias in multiferroic epitaxial heterostructures. *Phys. Rev. Lett.* **97**, 227201 (2006).
28. A. Scholl, F. Nolting, J. W. Seo, H. Ohldag, J. Stöhr, S. Raoux, J.-P. Locquet, J. Fompeyrine, Domain-size-dependent exchange bias in Co/$LaFeO_3$. *Appl. Phys. Lett.* **85**, 4085–4087 (2004).
29. L. W. Martin, Y.-H. Chu, Q. Zhan, R. Ramesh, S.-J. Han, S. X. Wang, M. Warusawithana, D. G. Schlom, Room temperature exchange bias and spin valves based on $BiFeO_3$/$SrRuO_3$/$SrTiO_3$/Si (001) heterostructures. *Appl. Phys. Lett.* **91**, 172513 (2007).
30. J. Allibe, S. Fusil, K. Bouzehouane, C. Daumont, D. Sando, E. Jacquet, C. Deranlot, M. Bibes, A. Barthélémy, Room temperature electrical manipulation of giant magnetoresistance in spin valves exchange-biased with $BiFeO_3$. *Nano Lett.*, **12**, 1141–1145 (2012).
31. S. M. Wu, S. A. Cybart, P. Yu, M. D. Rossell, J. X. Zhang, R. Ramesh, R. C. Dynes, Reversible electric control of exchange bias in a multiferroic field-effect device. *Nat. Mater.* **9**, 756–761 (2010).
32. X. He, Y. Wang, N. Wu, A. N. Caruso, E. Vescovo, K. D. Belashchenko, P. A. Dowben, C. Binek, Robust isothermal electric control of exchange bias at room temperature. *Nat. Mater.* **9**, 579–585 (2010).
33. L. D. Landau, E. M. Lifshitz, L. P. Pitaevskii, *Electrodynamics of Continuous Media: Vol. 8 of the Course of Theoretical Physics* (Elsevier, ed. 2, 2013).
34. S. Manipatruni, D. E. Nikonov, I. A. Young, Beyond CMOS computing with spin and polarization. *Nat. Phys.* **14**, 338–343 (2018).
35. J. T. Heron, D. G. Schlom, R. Ramesh, Electric field control of magnetism using $BiFeO_3$-based heterostructures. *Appl. Phys. Rev.* **1**, 021303 (2014).
36. J. J. Wang, J. M. Hu, T. N. Yang, M. Feng, J. X. Zhang, L. Q. Chen, C. W. Nan, Effect of strain on voltage-controlled magnetism in $BiFeO_3$-based heterostructures. *Sci. Rep.* **4**, 4553 (2014).

Acknowledgments

Funding: R.R. acknowledges support from the SRC-JUMP program through the ASCENT center. Y.-L.H. is supported by a grant from the DOE Advanced Manufacturing Office. B.P. is supported by a grant from Intel. S.M. acknowledges discussions with F. Rana. We also acknowledge K. Oguz, B. Buford, and T. Gosavi from Intel. **Author contributions:** S.M. designed the experiments, developed the analytical model for magnetoelectric LLG, and performed the electrical and magnetic measurements. B.P., Y.-L.H., Z.C., A.R.D., and R.R. deposited the stacks and performed materials development and metrology. C.-C.L. and S.M. developed the device layout. C.-C.L. designed and performed the process flow for ME devices on nonstandard substrates. D.E.N. performed the micromagnetic simulations for device scaling understanding. R.R. designed the material stacks and deposition

experiments and analyzed the experimental data. S.M., B.P., Y.-L.H., R.R., C.C., and I.A.Y. analyzed the experimental data. I.A.Y. supervised the whole project. S.M. wrote the manuscript supported by D.N., R.R., and I.A.Y. All authors participated in the manuscript edits.
Competing interests: S.M., C.-C.L., D.N., and I.A.Y. are employed at Intel Corporation. The other authors declare that they have no competing interests. **Data and materials availability:** All data needed to evaluate the conclusions in the paper are present in the paper and/or the Supplementary Materials. The micromagnetics code is appended to the Supplementary Materials. Additional data related to this paper may be requested from the authors.

Submitted 25 February 2018
Accepted 25 October 2018
Published 23 November 2018
10.1126/sciadv.aat4229

Citation: S. Manipatruni, D. E. Nikonov, C.-C. Lin, B. Prasad, Y.-L. Huang, A. R. Damodaran, Z. Chen, R. Ramesh, I. A. Young, Voltage control of unidirectional anisotropy in ferromagnet-multiferroic system. *Sci. Adv.* **4**, eaat4229 (2018).

Science Advances

Voltage control of unidirectional anisotropy in ferromagnet-multiferroic system

Sasikanth Manipatruni, Dmitri E. Nikonov, Chia-Ching Lin, Bhagwati Prasad, Yen-Lin Huang, Anoop R. Damodaran, Zuhuang Chen, Ramamoorthy Ramesh and Ian A. Young

Sci Adv **4** (11), eaat4229.
DOI: 10.1126/sciadv.aat4229